



OPEN

# Long-lived and Well-resolved Mn<sup>2+</sup> Ion Emissions in CuInS-ZnS Quantum Dots

SUBJECT AREAS:  
QUANTUM DOTS  
NANOPARTICLESSheng Cao<sup>1,2</sup>, Chengming Li<sup>1</sup>, Lin Wang<sup>2</sup>, Minghui Shang<sup>2</sup>, Guodong Wei<sup>2</sup>, Jinju Zheng<sup>2</sup> & Weiyu Yang<sup>2</sup><sup>1</sup>School of Materials Science and Engineering, University of Science and Technology Beijing, Beijing 100083, China, <sup>2</sup>Institute of Materials, Ningbo University of Technology, Ningbo 315016, China.Received  
27 August 2014Accepted  
14 November 2014Published  
17 December 2014Correspondence and  
requests for materials  
should be addressed to  
J.Z.  
(zhengzhao2007@  
163.com) or W.Y.  
(weiyuyang@  
tsinghua.org.cn)

CuInS<sub>2</sub> (CIS) quantum dots (QDs) have tunable photoluminescence (PL) behaviors in the visible and near infrared spectral range with markedly lower toxicity than the cadmium-based counterparts, making them very promising applications in light emitting and solar harvesting. However, there still remain material- and fabrication- related obstacles in realizing the high-performance CIS-based QDs with well-resolved Mn<sup>2+</sup> *d-d* emission, long emission lifetimes as well as high efficiencies. Here, we demonstrate the growth of high-quality Mn<sup>2+</sup>-doped CuInS-ZnS (CIS-ZnS) QDs based on a multi-step hot-injection strategy. The resultant QDs exhibit a well-resolved Mn<sup>2+</sup> *d-d* emission with a high PL quantum yield (QY) up to 66% and an extremely long excited state lifetime up to ~3.78 ms, which is nearly two times longer than the longest one of “green” QDs ever reported. It is promising that the synthesized Mn<sup>2+</sup>-doped CIS-ZnS QDs might open new doors for their practical applications in bioimaging and opto/electronic devices.

Manganese ions-doped (Mn<sup>2+</sup>-doped) semiconductor nanocrystals (NCs), as a lucrative alternative to semiconductor QDs, can not only maintain nearly all the intrinsic advantages of QDs, but also possess the additional merits such as larger Stokes shifts, enhanced thermal and chemical stabilities, as well as longer excited state lifetimes, which suggest their exciting and interesting applications in biomedical diagnosis, QD solar cells (QDSCs), light-emitting diodes (LEDs) and so forth<sup>1–4</sup>. Up to date, considerable interest has been attracted in the Mn<sup>2+</sup>-doped semiconductor NCs<sup>5–14</sup>. Even highly efficient Mn<sup>2+</sup> emissions have often been achieved in the binary intrinsic/alloyed group II–VI semiconductor NCs, these hosts are limited in either needing high energy for excitation<sup>11,12</sup> or containing the toxic elements of Cd and/or Se against the environment-friendly applications<sup>9,11,13</sup>.

Colloidal group I-III-VI NCs could offer a facility to tailor the bandgaps without the use of toxic elements, which might advance the exploration of high-performance “green” QDs<sup>15,16</sup>. Among the families of group I-III-VI semiconductors, CuInS<sub>2</sub> (CIS) has an intrinsic direct bandgap of 1.5 eV with size-dependent luminescence behaviors in the visible and near infrared range. Meanwhile, their bandgaps can be tailored widely by growing a ZnS shell or making them be alloyed CuZnInS (CZIS) NCs with Zn, to meet the prerequisite for the well-resolved Mn<sup>2+</sup> *d-d* emission, which can be expected to be the ideal “green” materials for widespread technological applications where the Mn<sup>2+</sup> emission required<sup>17–19</sup>. As compared to the CZIS alloyed QDs, the CIS-ZnS core-shell counterparts with the designed growth of ZnS shells, show the remarkable advantages to offer a significantly effective surface passivation for higher PL QYs<sup>19–24</sup>, as well a more facility to control the Mn<sup>2+</sup> positions<sup>25</sup>. For examples, Yang *et al.* reported the synthesis of Mn<sup>2+</sup>-doped CdS/ZnS core-shell NCs with Mn<sup>2+</sup> at controlled radial positions used a three-step synthesis route<sup>25</sup>. Liu *et al.* reported the Mn:CIS/ZnS core-shell QDs, which exhibited tunable PL peaked from 542 to 648 nm<sup>20</sup>, and Ding *et al.* also reported the CIS/Mn:ZnS QDs had high PL QY due to the effective surface passivation by ZnS shell<sup>26</sup>. It should point out that the defect state emission is predominantly in their PL spectra and no pure atomic-like Mn<sup>2+</sup> *d-d* emission was observed. Besides the improved high PL QY by the effective surface passivation, the lifetime of the PL has been considered as another important role on the performance of the QD nanodevices, since the long lifetime benefits to modifying the charge separation and recombination dynamics<sup>22,27</sup>. Luo *et al.* achieved a high power conversion efficiency (PCE) of 5.38% in the QDSCs with Mn:CIS/CdS core-shell QDs, showing a 14.7% higher PEC than CIS/CdS counterparts<sup>22</sup>. With respect to state-of-the-art CIS based QDs, regardless of the fact that even the Mn<sup>2+</sup> dopants did have been incorporated, there still remain material- and fabrication- related obstacles in realizing high-performance CIS-based QDs with well-resolved Mn<sup>2+</sup> *d-d* emission and high efficiency as well as long lifetimes<sup>15,28</sup>, which are important for their applications, *e.g.*, in bioimaging, opto/electronic devices.

Here, we report the synthesis of Mn<sup>2+</sup> doped CIS-ZnS QDs based on a multi-step hot-injection method. We mainly focus on three important topics for conferring the CIS-ZnS QDs with high optical performances: i) to



grow high-quality  $\text{Mn}^{2+}$ -doped CIS-ZnS QDs; ii) to obtain the well-resolved  $\text{Mn}^{2+}$  emission in CIS-ZnS QDs; iii) to make the long excited state lifetime of  $\text{Mn}^{2+}$  emission in CIS-ZnS QDs as well as high efficient PL QYs. The resultant CIS-ZnS QDs exhibit highly efficient and well-resolved  $\text{Mn}^{2+}$   $d$ - $d$  emission with a PL QY up to 66% and a surprisingly long lifetime up to  $\sim 3.78$  ms, which is nearly two times longer than the longest one of “green” QDs ever reported. We believe that the as-synthesized  $\text{Mn}^{2+}$ -doped CIS-ZnS QDs with high qualities might open new doors for their practical applications in bioimaging and opto/electronic devices.

## Methods

**Raw materials.** The materials of zinc stearate ( $\text{ZnSt}_2$ , ZnO 11.3–11.5%), cuprous chloride ( $\text{CuCl}$ , 99.999%), sulfur powder (S, 99.99%), 1-dodecanethiol (DDT, 98%), 1-octadecanethiol (ODT, 97%), oleylamine (OLA, 70%), manganese acetate ( $\text{Mn}(\text{Ac})_2$ ), and tetrabutylammonium hexafluorophosphate (98%) were commercially available from Aladdin company, China. 1-octadecene (ODE, 90%) was bought from Adamas-beta company, China. Indium (III) acetate ( $\text{In}(\text{Ac})_3$ , 99.99% trace metals basis) was purchased from Aldrich company, China. All the chemicals were used directly without further purification.

**Preparation of stock solutions.** S stock solutions were prepared by taking 6.4 mg S powders and 0.2 mL OLA into 1.5 mL ODE with gently heating under argon atmosphere. Zinc precursor solutions were prepared using 0.632 g  $\text{ZnSt}_2$ , 2 mL OLA and 2 mL DDT dissolved in 6 mL ODE. A typical manganese precursor solution was prepared by dissolving 5 mg  $\text{Mn}(\text{Ac})_2$  and 0.5 mL OLA in 1.5 mL ODE. Several types of manganese precursor solutions were prepared for growing  $\text{Mn}^{2+}$ -doped CuInS-ZnS QDs with tailored doping concentrations.

**Synthesis of  $\text{Mn}^{2+}$ -doped CuInS-ZnS QDs.** The  $\text{Mn}^{2+}$ -doped CuInS-ZnS QDs were synthesized by a hot-injection method with following three typical steps (as shown in Figure 1). Firstly, CIS cores were grown. Then the zinc precursors with various amounts of manganese precursor contents were injected into the solutions for the growth of a  $\text{Zn}_{1-x}\text{Mn}_x\text{S}$  shell around the CIS core. Subsequently, the ZnS shells were grown by introducing the stock solutions of zinc precursors, finally leading to the formation of  $\text{Mn}^{2+}$ -doped CIS-ZnS QDs. In a typical experimental procedure, 1 mg  $\text{CuCl}$ , 29 mg  $\text{In}(\text{Ac})_3$ , 2 mL DDT and 5 mL ODE were transferred into a 100 mL three necked flask, and degassed for 20 min by bubbling with Ar at  $150^\circ\text{C}$ . Then the S stock solution was injected quickly into the flask to form CIS nanoclusters. The solution was then annealed for 10 min, followed by being rapidly injected into 1 mL Zn stock solution and manganese precursor solution. At the meantime, the temperature was heated up to  $200^\circ\text{C}$ , and maintained there for 20 min to allow the growth of  $\text{Zn}_{1-x}\text{Mn}_x\text{S}$  shell. After that, the temperature was heated up to  $230^\circ\text{C}$ , and 8 mL Zn stock solution was then introduced into the reaction mixture in 4 batches at an interval of 20 min. The resultant colloidal solutions were cooled down naturally to room temperature, followed by purified repeatedly using methanol/hexanes and precipitated using acetone. To make the growth of the  $\text{Mn}^{2+}$ -doped CIS-ZnS QDs with various Cu/In ratios, the Mn dopant nominal concentration and the In precursor were kept at 2.25 mol% and 0.1 mmol, respectively, with otherwise same experimental procedures. For the synthesis of CIS-ZnS QDs with different Mn doping concentrations, the Cu/In nominal ratios were kept at 1/10 with otherwise same experimental procedures. The experimental results suggested that the production of the QDs *via* the present multi-step hot-injection strategy was highly repeatable.

**Structure characterization and optical property measurements.** The obtained QDs were characterized using high-resolution transmission electron microscopy (HRTEM, JEM-2100F, JEOL, Japan) equipped with energy dispersive X-ray spectroscopy (EDX, Quantax-STEM, Bruker, Germany), and X-ray diffraction (XRD, D8 Advance, Bruker, Germany). The average diameter of the  $\text{Mn}^{2+}$ -doped QDs was decided by the Scherrer's law:

$$d = \frac{K\lambda}{\beta \cos\theta} \quad (1)$$

Where  $K$  is a dimensionless shape factor (a typical value of 0.9 for spherical objects used as the first approximation),  $\beta$  is the full-width at half maxima (FWHM) of the peak, and  $\theta$  is the Bragg angle of the corresponding diffraction peak.

The UV-Vis measurements of the obtained QDs were performed on a UV-Vis scanning spectrophotometer (U-3900, Hitachi, Japan). The PL spectra, PL QY, and PL decay curves were recorded using a spectrometer (Fluoromax-4P, Horiba Jobin Yvon, France) equipped with a quantum-yield accessory and a time-correlated single-photon-counting (TCSPC) spectrometer. A pulsed xenon lamp and NanoLED (wavelength: 370 nm) were utilized as the exciting sources for PL decay measurements. The PL decay curves were analyzed using DAS6 software. The lifetime data was fitted by the biexponential function:

$$I = y_0 + A_1 \exp(-t/\tau_1) + A_2 \exp(-t/\tau_2) \quad (2)$$

Where  $\tau_1$  and  $\tau_2$  are the time constants, respectively,  $A_1$  and  $A_2$  are the normalized amplitudes of the components, respectively. The average lifetime was calculated by:

$$\tau_{ave} = \frac{A_1\tau_1^2 + A_2\tau_2^2}{A_1\tau_1 + A_2\tau_2} \quad (3)$$

The electron paramagnetic resonance (EPR) was taken on an X-band spectrometer (EPR, ER200-SRC, Bruker, Germany). The cyclic voltammograms (CV) were recorded on an electrochemical workstation (CHI600, Chenhua, China), using the glassy carbon disc, Pt wire and Ag/AgCl as the working, counter and reference electrodes, respectively. 0.1 M tetrabutylammonium hexafluorophosphate ( $\text{TBAPF}_6$ ) dissolved in acetonitrile was employed as the supporting electrolyte. The working electrodes were polished, cleaned, and dried before depositing the NC samples. Then a drop of diluted NC solution was deposited onto the surface of the working electrode to form a NC film. The scan rate was set at 50 mV/s. During all the experiments, the electrolyte solutions were thoroughly deoxygenated by bubbling nitrogen gas (99.99%).

## Results

### Structure and optical property of $\text{Mn}^{2+}$ -doped CIS-ZnS QDs.

Figure 2(a) shows a typical TEM image of  $\text{Mn}^{2+}$ -doped CIS-ZnS QDs. The QDs are nearly spherical (see also Supplementary Figure S1(a)), with a fairly monodisperse size distribution (the inset in Supplementary Figure S1(a)). The average size of these QDs is  $3.7 \pm 0.3$  nm, as determined from the TEM images. The lattice fringes are clear (Figure 2(b)), indicating the crystalline nature of the resultant QDs. Figure 2(c) shows the representative X-ray diffraction (XRD) patterns of the CIS-ZnS QDs with and without Mn dopants, indicating no apparent difference between them. The peaks are broadened, implying the tiny size of the resultant QDs. All the diffraction peaks are centered between those of CIS (JCPDS Card No. 471372) and ZnS (JCPDS Card No. 659585), clarifying that the QDs should be zinc blended phase of CIS-ZnS, rather than a mixture of CIS and ZnS. The average diameter of the QDs was *ca.* 3.6 nm based on the Debye-Scherrer formula by using the (111) diffraction within the XRD pattern, which is in good agreement with the TEM observations. The mean incorporated  $\text{Mn}^{2+}$  concentration (*i.e.*,  $\text{Mn}/(\text{Zn} + \text{Cu} + \text{In})$ ) is  $\sim 1.05$  mol% from the EDX measurement (see Supplementary Figure S2), which is lower than 2.25 mol% feed in the raw materials. The electron paramagnetic resonance (EPR) spectra also support the presence of  $\text{Mn}^{2+}$  in the doped NCs. Figure 2(d) presents a typical EPR spectrum of the as-synthesized  $\text{Mn}^{2+}$ -doped CIS-ZnS QDs. The hyperfine coupling constant ( $A$ ) of 63 Gauss

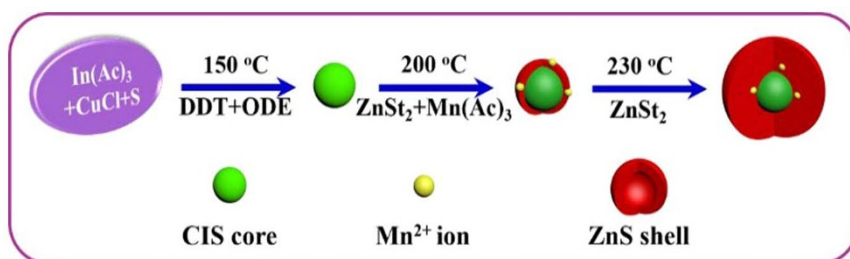


**Figure 1** | Schematic illustration for the growth of  $\text{Mn}^{2+}$ -doped CIS-ZnS QDs *via* the multi-step hot-injection strategy.

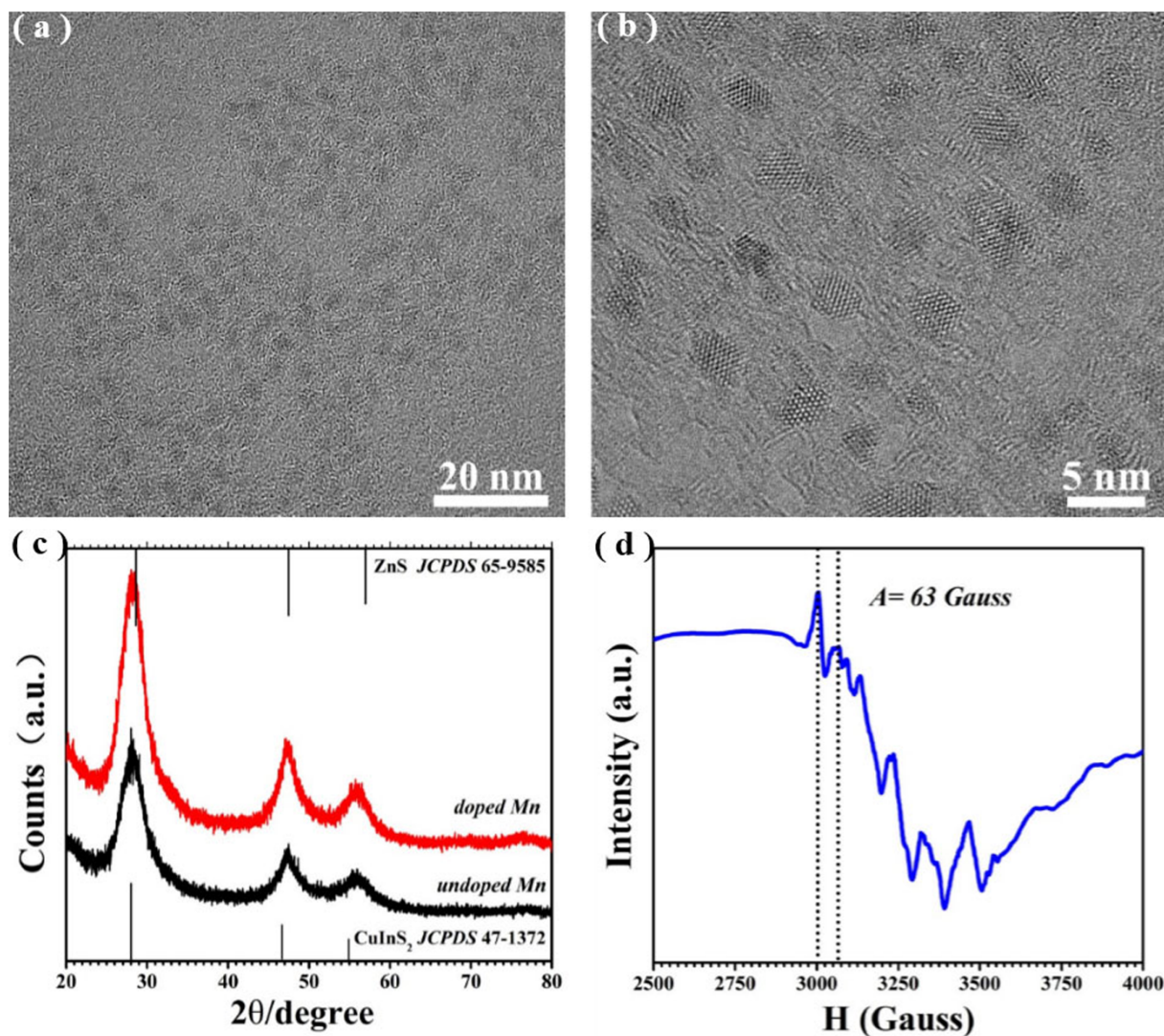


**Figure 2** | (a–b) Typical TEM images of the  $\text{Mn}^{2+}$ -doped CIS-ZnS QDs under different magnifications. (c) Typical XRD patterns of CIS-ZnS QDs with (red) and without (black)  $\text{Mn}^{2+}$  dopants. (d) Typical EPR spectrum of the  $\text{Mn}^{2+}$ -doped CIS-ZnS QDs by treatment with pyridine.

calculated from Figure 2(d), is very close to  $\text{Mn}^{2+}$  embedded in ZnS NC matrix (64.5 Gauss)<sup>29</sup>, suggesting that the  $\text{Mn}^{2+}$  ions have been successfully incorporated into the QDs. However, the broadening of the peak, rather than the six clear hyperfine splittings, is expected due to the complex environment of the Mn in the presence of copper<sup>19–21</sup>. We also noticed that the dipole-dipole interactions between the  $\text{Mn}^{2+}$  impurities can also broaden the EPR signal spectra<sup>7</sup>, which maybe together give rise to the broadening of the EPR signal spectra.

Figure 3 shows the typical absorption, PL, and PL excitation (PLE) spectra of the doped (*i.e.*, with 2.25 mol% nominal dopants) and undoped CIS-ZnS QDs. The absorption spectra have the similar onset at around 500 nm. The poorly resolved excitonic absorption is ascribed to the typical characteristic of the ternary and quaternary, which is partially caused by the special inhomogeneous composition distributions among different NCs<sup>15,16</sup>. Unlike the absorption spectra with the similar onset, the emission spectra are different, in which the peaks are centered at  $\sim 557$  and  $\sim 610$  nm for the undoped and doped QDs, respectively. The PL in the undoped CIS-ZnS QDs could be attributed to the host defect state emission<sup>15,16</sup>. The highly intense orange-yellow emission with a PL wavelength of  $\sim 610$  nm and the FWHM of  $\sim 80$  nm should result from the  ${}^4T_1-{}^6A_1$  transition of the  $\text{Mn}^{2+}$  impurity, which is excited by the energy transfer from the host CIS-ZnS, according to the similar onsets of PLE and absorption

spectra in Figure 3. The origin of the PL can also be confirmed by the surprisingly long excited-state lifetime (typically in a millisecond time scale) as discussed in the following section (Figure 4)<sup>4,10,13,30</sup>. What's more, the blue-shifted PL wavelengths in the temperature-dependent PL spectra are also a further indication for the  $\text{Mn}^{2+}$  emission. (see Supplementary Figure S3)<sup>4,31</sup>. Notably, such  $\text{Mn}^{2+}$ -doped CIS-ZnS QD gives a symmetric red emission centered at 610 nm (2.03 eV), which could be ascribed to the changed crystal field splitting in the coordination environments by the lattice mismatch between CIS cores and ZnS shells<sup>14</sup>. In addition, the PL FWHM ( $\sim 80$  nm) of these QDs is obviously much wider than that of a single Mn-doped CdS/ZnS QDs ( $\sim 20$  nm)<sup>32</sup>. This is mainly because that the Mn PL in the current case is an artifact of averaging over a large number of contributions from numerous QDs in different environments<sup>32</sup>. The PL QY of the host defect state emission is 40% for the undoped counterparts, while that of the  $\text{Mn}^{2+}$ -doped CIS-ZnS QDs can be up to 66% (the corresponding digital photographs are inset in Figure 3; details for the QY measurement, see Supplementary Figure S4), which is comparable to the best one of  $\text{Mn}^{2+}$ -doped semiconductor NCs ever reported.

Figure 4(a) and (b) show the corresponding PL decay curves of the  $\text{Mn}^{2+}$ -doped and undoped CIS-ZnS QDs at room temperature, respectively. In contrast to undoped QDs with a short PL lifetime

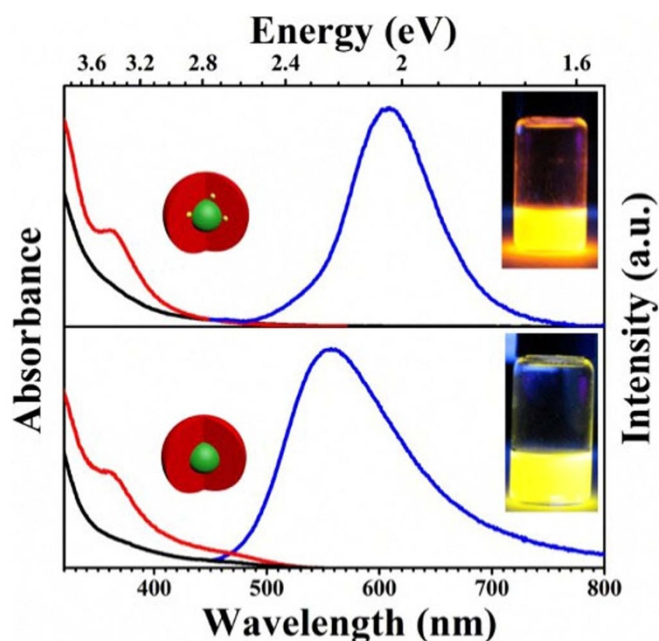


**Figure 3** | Typical UV-Vis absorption (black), PLE (red), and PL (blue) spectra of the as-synthesized  $\text{Mn}^{2+}$ -doped (upper) and undoped (below) CIS-ZnS QDs at room temperature. The insets show their corresponding digital photos of these QDs under UV light illumination excited at a wavelength of 365 nm.

often scaled in nanosecond, the  $\text{Mn}^{2+}$ -doped QDs exhibits a much longer lifetime in a millisecond scale. For the doped CIS-ZnS QDs, to clearly present the decay dynamics, the same data in the low time regime is shown as the inset in Figure 4a. To further compare the decay characteristics between the doped and undoped QDs, their decay curves are plotted in the low time regime from 0 to 4000 ns, which is shown as the inset in Figure 4b. This suggests that the decay of the doped sample is obviously beyond the window of 4000 ns. However, the PL intensity of the undoped counterparts becomes basically invariable after 3000 ns (the residual signals are attributed to the noise). Furthermore, the PL intensity of the undoped QDs decays much quicker than that of the doped sample. These experimental results suggest that there is not obvious overlapping of surface states with the Mn emission in the doped sample. These PL decay lines are fitted by a biexponential function, and their time constants and normalized amplitudes are summarized in the Table 1, respectively. As seen in this table, the average lifetimes are 3.78 ms and 401 ns for doped and undoped QDs, respectively. To the best of our knowledge, such excited-state lifetime of  $\sim 3.78$  ms is a new record of the longest one for all the “green”  $\text{Mn}^{2+}$ -doped QDs, which is nearly two times longer than the longest one previously reported (*i.e.*,  $\sim 2.12$  ms<sup>19</sup>).

**Effect of the Cu/In ratios on the  $\text{Mn}^{2+}$  emission in  $\text{Mn}^{2+}$ -doped CIS-ZnS QDs.** Figure 5 shows the evolution of PL spectra of  $\text{Mn}^{2+}$ -doped CIS-ZnS QDs starting from the CIS cores (the nominal Mn doping concentration and In precursor are kept constants at 2.25 mol% and 0.1 mmol, respectively), which were prepared with the Cu/In nominal molar ratios of 1/2, 3/10, and 1/10, corresponding to Figure 5(a), (b) and (c), respectively. As seen in Figure 5(a) and (b) with the Cu/In nominal molar ratios of 1/2 and 3/10, the overgrowth with  $\text{Zn}_{1-x}\text{Mn}_x\text{S}$  and/or ZnS shell typically leads to a systematical blue shift of the PL spectra, which likely indicates the etching of the core material under the shell growth conditions and associated increase in the degree of the spatial confinement<sup>12,16,33</sup>. Nonetheless, even the  $\text{Mn}^{2+}$  ions have been incorporated into the

NCs, it should be noted that there is no detectable  $\text{Mn}^{2+}$  emission, since their PL lifetimes scaled in nanosecond (see Supplementary Figure S5). However, for the sample with a reduced Cu/In nominal molar ratio of 1/10 (Figure 5(c)), after the ZnS shell deposition, the well-resolved  $\text{Mn}^{2+}$  emission could be achieved. The PL peak wavelengths cannot be further tuned although its intensity is still enhanced with the reactions progressed. In addition, the PL spectra are relatively narrower in contrast to those of the samples with higher Cu/In nominal ratios of 1/2 and 3/10. These observations clearly indicate that the Cu/In ratios play a key role for obtaining the well-resolved  $\text{Mn}^{2+}$  *d-d* emission in the CIS-ZnS QDs. As we known, the decrease of the Cu/In molar ratio will increase the bandgap of CIS cores since  $\text{In}_2\text{S}_3$  (2.07 eV) and InS (2.44 eV) have wider bandgaps than  $\text{Cu}_2\text{S}$  (1.2 eV)<sup>34,35</sup>, which are also confirmed by the blue shifts of the absorption band edge (see Supplementary Figure S6) with a reduced Cu/In ratio and the cyclic voltammetry (C-V) investigations (see Supplementary Figure S7). The host bandgaps are estimated to be  $\sim 2.0$ , 2.1 and 2.3 eV from the absorption and C-V lines for the  $\text{Mn}^{2+}$ -doped CIS-ZnS QDs grown with the Cu/In nominal ratios of 1/2, 3/10, and 1/10, respectively. Considering the fact that  $\text{Mn}^{2+}$  emission can only occur in the QDs with a wider host bandgap over than the  $\text{Mn}^{2+}$  ligand field transition energy<sup>36,37</sup>, this suggests that the host bandgap can reach or exceed the  $\text{Mn}^{2+}$  ligand field transition energy ( $\sim 2.03$  eV for our  $\text{Mn}^{2+}$ -doped CIS-ZnS QDs) with the decreased Cu/In ratio. This might clarify the absence of  $\text{Mn}^{2+}$  emission from the  $\text{Mn}^{2+}$ -doped CIS-ZnS QDs in the reported works, since the Cu/In molar ratios were generally much higher than  $1/10$ <sup>21,23,26</sup>. We also noticed that, for Mn and Cu co-doped QDs, the Cu emission is dominant with suppressing Mn-related emission when the distance between Cu and Mn ions is close enough<sup>38</sup>. This accounts for the suppression of the  $\text{Mn}^{2+}$  emission in the sample with the Cu/In nominal ratio of 3/10, since the bandgap is marginally larger than the  $\text{Mn}^{2+}$  ligand field transition energy. In other words, the Cu/In molar ratios play a key role for obtaining the  $\text{Mn}^{2+}$  *d-d* emission, and a reduced Cu/In molar ratio favors the presence of the well-resolved  $\text{Mn}^{2+}$  emission in CIS-ZnS QDs.

**Effect of the  $\text{Mn}^{2+}$  doping concentrations on the spectral characteristics in  $\text{Mn}^{2+}$ -doped CIS-ZnS QDs.** Figure 6 presents the effects of the nominal  $\text{Mn}^{2+}$  doping concentrations (*i.e.* 0–2.25 mol%) on the spectral characteristics of CIS-ZnS QDs with the Cu/In nominal molar ratio kept at 1/10. The FWHM of the PL spectrum becomes narrower with the increase of the  $\text{Mn}^{2+}$  doping concentrations, suggesting that the wide band PL of the QDs with a low  $\text{Mn}^{2+}$  concentration maybe originates from both host defect state emission and dopant  $\text{Mn}^{2+}$  emission. The time-resolved spectroscopy measurements are undertaken to distinguish the origin of the emission for the QDs (see Supplementary Figure S8). The obviously narrowed PL spectrum after the delay for the QDs with a lower  $\text{Mn}^{2+}$  concentration (*i.e.* 0.75 mol%) confirms the combined origin of the PL. Meanwhile, the similar normalized time-resolved PL spectra with various delay times for the sample with a higher Mn concentration (*i.e.* 2.25 mol%) disclose that the doped QDs possess a basically pure  $\text{Mn}^{2+}$  *d-d* emission. The experimental results imply that the emission in the present QDs can be controlled by tailoring the amounts of Mn dopants<sup>7,8,39</sup>. The increased Mn concentration will result in the decreased proportion of the host defect state emission in the PL spectra, and the well-resolved  $\text{Mn}^{2+}$  *d-d* emission can be obtained at a nominal doping concentration of 2.25% in our case.

## Discussion

The growth of CIS-ZnS QDs in current work with a core-shell structure, rather than a homogeneous CZIS alloyed one and other side binary product, could be supported by following issues:

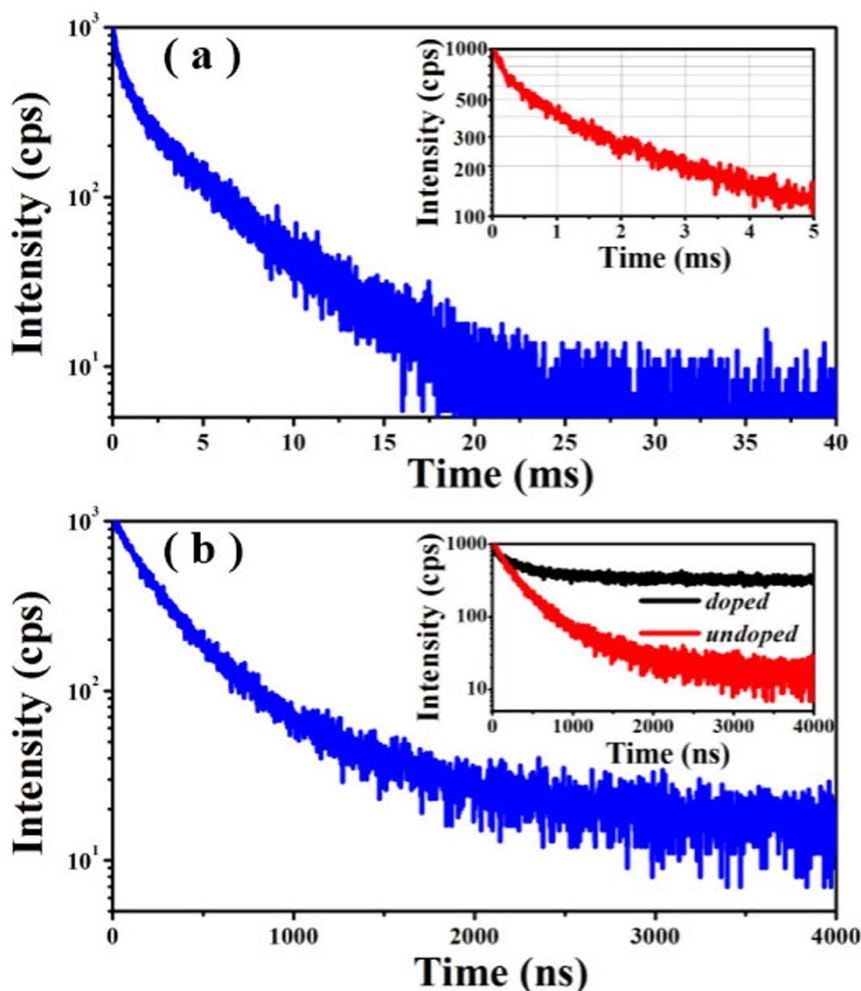


**Figure 4** | (a) Typical PL decay spectrum of  $\text{Mn}^{2+}$ -doped CIS-ZnS QDs. The up-right inset shows the same data in the low time regime. (b) Typical PL decay spectrum of  $\text{Mn}^{2+}$ -undoped CIS-ZnS QDs. The inset is the PL decay curves of  $\text{Mn}^{2+}$ -doped and undoped CIS-ZnS QDs in the same time range window.

- i) From the point of synthesis procedure. As reported in the previous works, the homogeneous alloyed QDs were often obtained *via* a one-pot method that all of precursors are introduced together at one time<sup>17,40</sup>. Different from the one-pot route, the multi-step hot-injection strategy (similar to our case, see the Experimental Procedure) often favors the growth of the QDs with a unique core-shell structure. For example, Park *et al.* have detailedly studied the overgrowth process of ZnS shell on  $\text{CuInS}_2$  cores to understand the obtained structure of CIS-ZnS QDs, which concluded that the CIS cores are not homogeneous alloy but a gradient composition after overcoated ZnS shell, namely the typical core-shell structures<sup>41</sup>. In our case, the temperature for the overgrowth of ZnS shell is identical to that in the literature as mentioned above (*i.e.* 230°C), which leads to the formation of the CIS-ZnS QDs in a typical core-shell structure<sup>41–45</sup>. After growth of the ZnS shells, the diameter of the CIS/ $\text{Zn}_{1-x}\text{Mn}_x\text{S}$  QDs is increased from  $2.8 \pm 0.3$  nm (Figure S1(b)) to  $3.7 \pm 0.3$  nm. Meanwhile, the corresponding XRD pattern also showed an obvious peak shift (see Figure S9, Supplementary Information). These facts indicate that the ZnS shells have been overcoated on the CIS/ $\text{Zn}_{1-x}\text{Mn}_x\text{S}$  cores. Thus, we deduced that, in the present work, the growth of CIS-ZnS QDs should be in a core-shell structure rather than a homogeneous alloyed one.
- ii) From the point of band gap. According to the reported work of alloyed  $(\text{CuInS}_2)_x(\text{ZnS})_{1-x}$  NCs by Pan *et al.*, the band gaps of these alloyed NCs with zinc blended phase can be tuned in the broad range from 1.5 to 3.7 eV by changing the ratios of  $\text{CuInS}_2$  to ZnS<sup>17</sup>. In our case, the Cu/In/Zn mole ratio is  $\sim 1/4/30$  (see Figure S2, Supplementary Information). If the homogeneous alloy structures were formed, the bandgap of the doped-QDs should be  $\sim 3.3$  eV. However, the host bandgap is estimated to be 2.3 eV from the absorption and C-V lines of our QDs, suggesting that our obtained QDs are not a homogeneous alloy structure.
- iii) From the PL spectral characteristics. It has been proposed that the preparation of CIS-ZnS QDs has a great challenge to balance

**Table 1** | Fitting parameters of PL dynamics of  $\text{Mn}^{2+}$  doped and undoped CIS-ZnS QDs

Sample	$A_1$	$\tau_1$	$A_2$	$\tau_1$	$\chi^2$	$\tau_{\text{ave}}$
Mn-doped	0.576	0.62 ms	0.424	4.39 ms	1.102	3.78 ms
undoped	0.785	198 ns	0.215	700 ns	1.036	401 ns

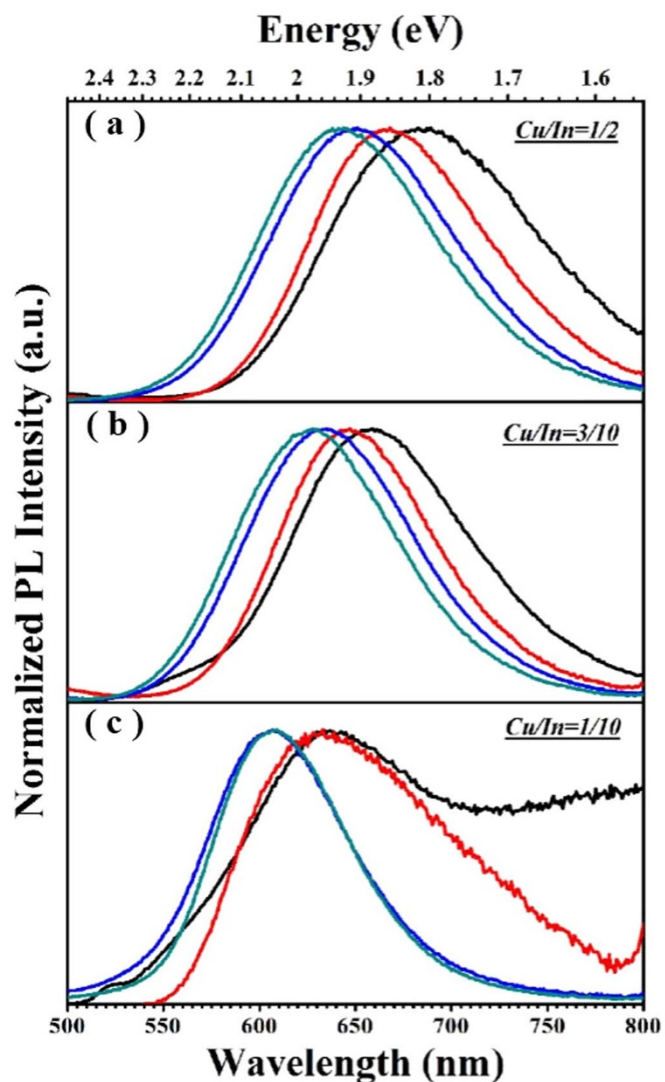


**Figure 5** | (a–c) Evolution of the PL spectra of  $\text{Mn}^{2+}$ -doped CIS-ZnS QDs with the overcoating of ZnS shells. The black lines in (a–c) refer to the PL spectrum evolutions of the CIS cores fabricated at the Cu/In ratios of 1/2, 3/10 and 1/10, respectively; The red lines in (a–c) refer to the PL spectrum evolutions of the QDs after the growth of a  $\text{Zn}_{1-x}\text{Mn}_x\text{S}$  layer around the CIS core by injecting the zinc + manganese precursor contents (0.1 mmol  $\text{ZnSt}_2$  + 0.03 mmol  $\text{Mn}(\text{Ac})_2$ ); The blue and cyan lines refer to the PL spectrum evolutions of the QDs after the growth of ZnS shells by introducing zinc precursors of 0.2  $\text{ZnSt}_2$  and 0.8 mmol  $\text{ZnSt}_2$ , respectively.

the reactivity of the metallic cations each other, in which the unfavorable phase separation will bring a mixture of binary products. Usually, for the  $\text{Mn}^{2+}$ -doped QDs, the  $\text{Mn}^{2+}$  emission is very sensitive to the located matrix environments<sup>13,46</sup>, which offers us a method to confirm the main products of the as-synthesized samples. Figure 7 shows the two-dimensional PL excitation (2d PLE) spectra of the synthesized QDs, which is obtained by measuring the PL spectra over a range of excitation energies containing the information of PLE and PL spectra. As shown in Figure 7, these  $\text{Mn}^{2+}$ -doped QDs can be excited even with 440 nm wavelength light, indicating that the  $\text{Mn}^{2+}$  *d-d* emission should be mainly excited by the energy transfer from the target multiple CIS-ZnS host, rather than some possible side products such as Mn:ZnS (at least not completely, since the bandgap of ZnS ( $\sim 3.7$  eV) is much larger than the excitation onset of the QDs). Furthermore, the PL spectra possess basically

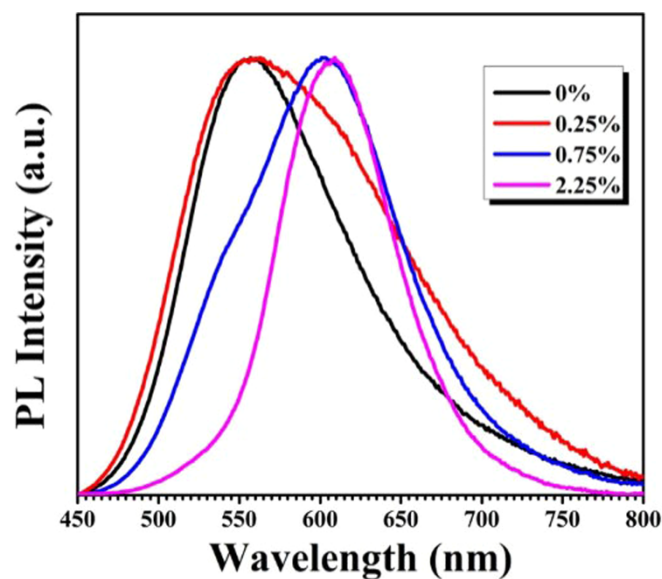


**Figure 6** | Representative PL spectra of  $\text{Mn}^{2+}$  doped CIS-ZnS QDs with different Mn initial concentrations at an excitation wavelength of 365 nm.

similar peak wavelengths at  $\sim 610$  nm when excited at the wavelengths ranged from 320 to 460 nm, which indicate that the local environment of emission centers should be homogeneous CIS-ZnS host rather than ZnS QDs, since the PL of the Mn:ZnS QDs is generally centered at  $\sim 580$  nm. In addition, the PLE spectra (see Supplementary Figure S10) for the  $\text{Mn}^{2+}$ -doped QDs taken at the different emission peak wavelengths are overlapped with each other, implying that the emission originates from the same particle set rather than from the extraneous species or undesired secondary formed QDs during the synthesis procedure. Thus, it could be confirmed that the as-synthesized product is  $\text{Mn}^{2+}$ -doped CIS-ZnS QDs rather than any other side binary products.

It is widely considered that a long excited state lifetime is one of the key factors for the design and development of the QDs nanodevices

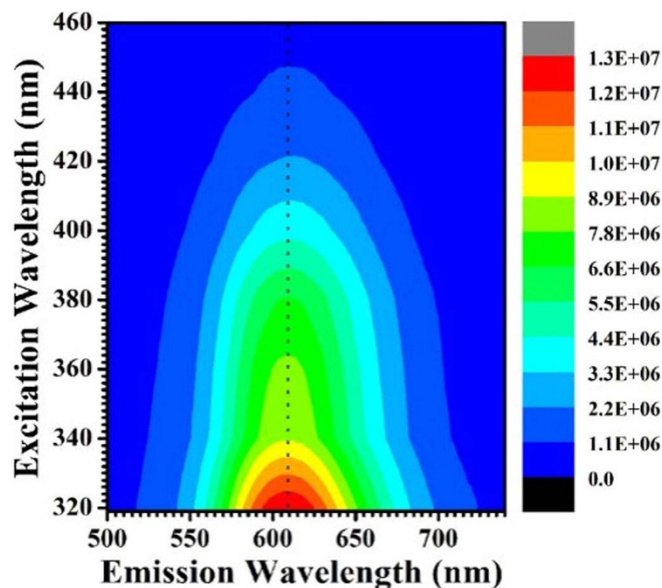


**Figure 7** | Representative 2d PLE spectra of  $\text{Mn}^{2+}$ -doped CIS-ZnS QDs. The PL intensities are represented by the colors.



Table 2 | Optical properties of Mn-doped QDs in the reported works

QDs	PL QY/(%)	Peak/(nm)	Lifetime/(ms)	Ref.
Mn:ZnS	65	585		12
Mn:ZnS	>50	585	0.37	47
Mn:ZnS	>50	590	1.71	10
MnS/ZnS/CdS	68	580	0.68	13
Mn:CdS/ZnS	56	585		25
Mn:ZnSe	80	585		48
Mn:ZnSe			2	49
Mn:ZnSe	40–60	585		11
Mn:CuInZnS	45	600	2.12	19
Mn:CuInS/ZnS	66	610	3.78	The present work

(e.g., bioimaging and QDSC)<sup>3,22,27</sup>. A longer excited-state carrier lifetime can not only facilitate the charge separation in QDSC, but also favor to eliminating the signal interference from the short life material in bioimaging. Table 2 summarizes the state-of-the-art Mn<sup>2+</sup> doped QDs in the reported works, suggesting that most of their PL QYs are typically lower than 60%. Furthermore, it should be worthwhile that these Mn<sup>2+</sup> doped QDs hosts either require high excitation energies (>3.6 eV), or contain the toxic elements such as Cd and/or Se, which are listed as a Class A elements against the environment-friendly applications. However, our Mn<sup>2+</sup>-doped CIS-ZnS core-shell QDs have a narrower host bandgap without toxic element Cd and/or Se. Most importantly, besides to their high PL QY up to 66% and well-resolved Mn<sup>2+</sup> emission, the present CIS-ZnS QDs possess an extremely long excited state lifetime up to 3.78 ms, which is the longest one ever reported. This is mainly attributed to the high-quality of CIS-ZnS QDs with a favorable Cu/In ratio and Mn<sup>2+</sup> doping concentration.

## Conclusions

In summary, we have demonstrated the growth of high-quality Mn<sup>2+</sup>-doped CIS-ZnS QDs based on a multi-step hot-injection method. The Cu/In molar ratios play a key role for obtaining the Mn<sup>2+</sup> *d-d* emission, and a reduced Cu/In molar ratio favors the well-resolved Mn<sup>2+</sup> emission in CIS-ZnS QDs. The increased Mn concentration will result in the decreased proportion of the host defect-trap emission in the PL spectra, and the well-resolved Mn<sup>2+</sup> *d-d* emission can be obtained at a favorable doping concentration. The resultant CIS-ZnS QDs exhibit a well-resolved Mn<sup>2+</sup> *d-d* emission with a high PL QY up to 66% and an extremely long excited state lifetime up to ~3.78 ms, which is nearly two times longer than the longest one of “green” QDs ever reported. It is believed that the as-fabricated “green” QDs in current work, with such extremely-long radiative excited-state lifetime and high efficiency, could be an excellent candidate for the practical applications in biological/biomedicine and opto/electronic devices.

- Beaulac, R., Schneider, L., Archer, P. I., Bacher, G. & Gamelin, D. R. Light-induced spontaneous magnetization in doped colloidal quantum dots. *Science* **325**, 973–976 (2009).
- Dai, Q., Sabio, E. M., Wang, W. & Tang, J. Pulsed laser deposition of Mn doped CdSe quantum dots for improved solar cell performance. *Appl. Phys. Lett.* **104**, 183901 (2014).
- Wu, P. & Yan, X. P. Doped quantum dots for chemo/biosensing and bioimaging. *Chem. Soc. Rev.* **42**, 5489–5521 (2013).
- Yuan, X. *et al.* Thermal stability of Mn<sup>2+</sup> ion luminescence in Mn-doped core-shell quantum dots. *Nanoscale* **6**, 300–307 (2014).
- Bhargava, R., Gallagher, D., Hong, X. & Nurmikko, A. Optical properties of manganese-doped nanocrystals of ZnS. *Phys. Rev. Lett.* **72**, 416–419 (1994).
- Sapra, S., Prakash, A., Ghangrekar, A., Periasamy, N. & Sarma, D. Emission properties of manganese-doped ZnS nanocrystals. *J. Phys. Chem. B* **109**, 1663–1668 (2005).
- Nag, A. *et al.* A study of Mn<sup>2+</sup> doping in CdS nanocrystals. *Chem. Mater.* **19**, 3252–3259 (2007).

- Nag, A., Chakraborty, S. & Sarma, D. To dope Mn<sup>2+</sup> in a semiconducting nanocrystal. *J. Am. Chem. Soc.* **130**, 10605–10611 (2008).
- Acharya, S., Sarma, D. D., Jana, N. R. & Pradhan, N. An alternate route to high-quality ZnSe and Mn-doped ZnSe nanocrystals. *J. Phys. Chem. Lett.* **1**, 485–488 (2010).
- Zheng, J. *et al.* Improved photoluminescence of MnS/ZnS core/shell nanocrystals by controlling diffusion of Mn ions into the ZnS shell. *J. Phys. Chem. C* **114**, 15331–15336 (2010).
- Zeng, R., Zhang, T., Dai, G. & Zou, B. Highly emissive, color-tunable, phosphine-free Mn:ZnSe/ZnS core/shell and Mn:ZnSe shell-alloyed doped nanocrystals. *J. Phys. Chem. C* **115**, 3005–3010 (2011).
- Zhang, W., Li, Y., Zhang, H., Zhou, X. & Zhong, X. Facile synthesis of highly luminescent Mn-doped ZnS nanocrystals. *Inorg. Chem.* **50**, 10432–10438 (2011).
- Cao, S. *et al.* Highly efficient and well-resolved Mn<sup>2+</sup> ion emission in MnS/ZnS/CdS quantum dots. *J. Mater. Chem. C* **1**, 2540–2547 (2013).
- Hazarika, A., Pandey, A. & Sarma, D. D. Rainbow Emission from an Atomic Transition in Doped Quantum Dots. *J. Phys. Chem. Lett.* **5**, 2208–2213 (2014).
- Aldakov, D., Lefrançois, A. & Reiss, P. Ternary and quaternary metal chalcogenide nanocrystals: synthesis, properties and applications. *J. Mater. Chem. C* **1**, 3756–3776 (2013).
- Zhong, H., Bai, Z. & Zou, B. Tuning the luminescence properties of colloidal I-III-VI semiconductor nanocrystals for optoelectronics and biotechnology applications. *J. Phys. Chem. Lett.* **3**, 3167–3175 (2012).
- Pan, D. *et al.* Alloyed semiconductor nanocrystals with broad tunable band gaps. *Chem. Commun.* **28**, 4221–4223 (2009).
- Beaulac, R. *et al.* Spin-polarizable excitonic luminescence in colloidal Mn<sup>2+</sup>-doped CdSe quantum dots. *Nano Lett.* **8**, 1197–1201 (2008).
- Manna, G., Jana, S., Bose, R. & Pradhan, N. Mn-doped multinary CIZS and AIZS nanocrystals. *J. Phys. Chem. Lett.* **3**, 2528–2534 (2012).
- Liu, Q., Deng, R., Ji, X. & Pan, D. Alloyed Mn-Cu-In-S nanocrystals: a new type of diluted magnetic semiconductor quantum dots. *Nanotechnology* **23**, 255706 (2012).
- Lin, B. *et al.* Multifunctional manganese-doped core-shell quantum dots for magnetic resonance and fluorescence imaging of cancer cells. *New J. Chem.* **37**, 3076–3083 (2013).
- Luo, J. *et al.* Highly efficient core-shell CuInS<sub>2</sub>-Mn doped CdS quantum dot sensitized solar cells. *Chem. Commun.* **49**, 3881–3883 (2013).
- Hua, J. *et al.* Photoluminescence properties of Cu-Mn-In-S/ZnS core/shell quantum dots. *Superlattices Microstruct.* **73**, 214–223 (2014).
- Sitbon, G. *et al.* Multimodal Mn-doped I-III-VI quantum dots for near infrared fluorescence and magnetic resonance imaging: from synthesis to in vivo application. *Nanoscale* **6**, 9264–9272 (2014).
- Yang, Y., Chen, O., Angerhofer, A. & Cao, Y. C. Radial-position-controlled doping in CdS/ZnS core/shell nanocrystals. *J. Am. Chem. Soc.* **128**, 12428–12429 (2006).
- Ding, K., Jing, L., Liu, C., Hou, Y. & Gao, M. Magnetically engineered Cd-free quantum dots as dual-modality probes for fluorescence/magnetic resonance imaging of tumors. *Biomaterials* **35**, 1608–1617 (2014).
- Santra, P. K. & Kamat, P. V. Mn-doped quantum dot sensitized solar cells: a strategy to boost efficiency over 5%. *J. Am. Chem. Soc.* **134**, 2508–2511 (2012).
- Lin, J. *et al.* Atomically precise doping of monomanganese ion into coreless supertetrahedral chalcogenide nanocluster inducing unusual red shift in Mn<sup>2+</sup> emission. *J. Am. Chem. Soc.* **136**, 4769–4779 (2014).
- Yang, B., Shen, X., Zhang, H., Cui, Y. & Zhang, J. Luminescent and magnetic properties in semiconductor nanocrystals with radial-position-controlled Mn<sup>2+</sup> doping. *J. Phys. Chem. C* **117**, 15829–15834 (2013).
- Zheng, J. *et al.* Efficient photoluminescence of Mn<sup>2+</sup> ions in MnS/ZnS core/shell quantum dots. *J. Phys. Chem. C* **113**, 16969–16974 (2009).
- Zheng, J. *et al.* Temperature-dependent photoluminescence properties of Mn:ZnCdS quantum dots. *RSC Adv.* **4**, 30948–30952 (2014).
- Hazarika, A. *et al.* Ultranarrow and widely tunable Mn<sup>2+</sup>-induced photoluminescence from single Mn-doped nanocrystals of ZnS-CdS alloys. *Phys. Rev. Lett.* **110**, 267401 (2013).



33. Chen, B. *et al.* Highly emissive and color-tunable CuInS<sub>2</sub>-based colloidal semiconductor nanocrystals: off-stoichiometry effects and improved electroluminescence performance. *Adv. Funct. Mater.* **22**, 2081–2088 (2012).
34. Kim, Y. *et al.* Synthesis of Au-Cu<sub>2</sub>S core-shell nanocrystals and their photocatalytic and electrocatalytic activity. *J. Phys. Chem. C* **114**, 22141–22146 (2010).
35. Khanchandani, S., Kundu, S., Patra, A. & Ganguli, A. K. Band Gap Tuning of ZnO/In<sub>2</sub>S<sub>3</sub> core/shell nanorod arrays for enhanced visible-light-driven photocatalysis. *J. Phys. Chem. C* **117**, 5558–5567 (2013).
36. Pradhan, N. & Sarma, D. Advances in light-emitting doped semiconductor nanocrystals. *J. Phys. Chem. C Lett.* **2**, 2818–2826 (2011).
37. Beaulac, R., Archer, P. I., Ochsenein, S. T. & Gamelin, D. R. Mn<sup>2+</sup>-doped CdSe quantum dots: new inorganic materials for spin-electronics and spin-photonics. *Adv. Funct. Mater.* **18**, 3873–3891 (2008).
38. Panda, S. K., Hickey, S. G., Demir, H. V. & Eychmuller, A. Bright white-light emitting manganese and copper co-doped ZnSe quantum dots. *Angew. Chem. Int. Ed.* **50**, 4432–4436 (2011).
39. Yang, H. & Holloway, P. H. Enhanced photoluminescence from CdS:Mn/ZnS core/shell quantum dots. *Appl. Phys. Lett.* **82**, 1965–1967 (2003).
40. Zhang, J., Xie, R. & Yang, W. A simple route for highly luminescent quaternary Cu-Zn-In-S nanocrystal emitters. *Chem. Mater.* **23**, 3357–3361 (2011).
41. Park, J. & Kim, S. W. CuInS<sub>2</sub>/ZnS core/shell quantum dots by cation exchange and their blue-shifted photoluminescence. *J. Mater. Chem.* **21**, 3745–3750 (2011).
42. Pons, T. *et al.* Cadmium-free CuInS<sub>2</sub>/ZnS quantum dots for sentinel lymph node imaging with reduced toxicity. *ACS Nano* **4**, 2531–2538 (2010).
43. Li, L. *et al.* Highly luminescent CuInS<sub>2</sub>/ZnS core/shell nanocrystals: cadmium-free quantum dots for in vivo imaging. *Chem. Mater.* **21**, 2422–2429 (2009).
44. Guo, W. Synthesis of Zn-Cu-In-S/ZnS core/shell quantum dots with inhibited blue-shift photoluminescence and applications for tumor targeted bioimaging. *Theranostics* **3**, 99 (2013).
45. Deng, D. *et al.* High-quality CuInS<sub>2</sub>/ZnS quantum dots for in vitro and in vivo bioimaging. *Chem. Mater.* **24**, 3029–3037 (2012).
46. Pradhan, N., Battaglia, D. M., Liu, Y. & Peng, X. Efficient, stable, small, and water-soluble doped ZnSe nanocrystal emitters as non-cadmium biomedical labels. *Nano Lett.* **7**, 312–317 (2007).
47. Srivastava, B. B. *et al.* Highly luminescent Mn-doped ZnS nanocrystals: gram-scale synthesis. *J. Phys. Chem. Lett.* **1**, 1454–1458 (2010).
48. Menkara, H. *et al.* Development of nanophosphors for light emitting diodes. *Opt. Express* **19**, A972–A981 (2011).
49. Weaver, A. L. & Gamelin, D. R. Photoluminescence brightening via electrochemical trap passivation in ZnSe and Mn<sup>2+</sup>-doped ZnSe quantum dots. *J. Am. Chem. Soc.* **134**, 6819–6825 (2012).

## Acknowledgments

This work was financially supported by National Natural Science Foundation of China (NSFC, Grant No. 61106066), 973 Program (Grant No. 2012CB326407) and Zhejiang Provincial Science Foundation (Grant No. LY14F040001).

## Author contributions

J.Z., C.L. and W.Y. conceived and directed the experiments. S.C., L.W., M.S. and G.W. performed the experiments. S.C., J.Z. and W.Y. co-wrote the manuscript. All authors discussed the results and helped with the preparation of the final manuscript.

## Additional information

**Supplementary information** accompanies this paper at <http://www.nature.com/scientificreports>

**Competing financial interests:** The authors declare no competing financial interests.

**How to cite this article:** Cao, S. *et al.* Long-lived and Well-resolved Mn<sup>2+</sup> Ion Emissions in CuInS-ZnS Quantum Dots. *Sci. Rep.* **4**, 7510; DOI:10.1038/srep07510 (2014).



This work is licensed under a Creative Commons Attribution-NonCommercial-ShareAlike 4.0 International License. The images or other third party material in this article are included in the article's Creative Commons license, unless indicated otherwise in the credit line; if the material is not included under the Creative Commons license, users will need to obtain permission from the license holder in order to reproduce the material. To view a copy of this license, visit <http://creativecommons.org/licenses/by-nc-sa/4.0/>